Dynamics of Ganglioside Headgroup in Lipid Environment: Molecular Dynamics Simulations of GM1 Embedded in Dodecylphosphocholine Micelle

Sheeja V. Vasudevan and Petety V. Balaji*

Biotechnology Center, Indian Institute of Technology, Bombay, Powai, Mumbai 400 076, India

Received: August 2, 2000; In Final Form: March 28, 2001

Recognition of membrane-anchored glycosphingolipid receptors by various ligands is the key event in several biological phenomena. However, mere presence of these cell-surface receptors does not always ensure their recognition and binding by their respective ligands, a phenomenon termed "crypticity". Earlier studies have suggested that different glycan headgroup orientations exposing and/or masking different epitopes may explain the crypticity of glycolipids. The effect of lipid environment on the orientation and conformation of GM1 ganglioside has been investigated in the present study by MD simulation technique in an attempt to understand the structural basis of crypticity. In addition, the effect of the length of the ceramide hydrocarbon tails on the headgroup conformation has also been investigated. MD simulations for 1 ns were performed with explicit water molecules for both GM1 headgroup (GM1-Os) and GM1 embedded in dodecylphosphocholine micelle. The simulations show that the conformations of the hydrocarbon tails, ceramide−saccharide linkages, and the headgroup are inter-related and are affected by micellar packing considerations. The conformations of GalNAc-β1→4-Gal and Neu5Ac-α2→3-Gal linkages were found to be restricted when GM1 is embedded in the micelle compared to that in GM1-Os. The GalNAc-β1→4-Gal linkage being a branch point, affects the orientation/accessibility of all the residues linked to GalNAc. If such a disallowed glycan conformation is necessary for recognition by, and binding to, their ligands, then the glycans may become cryptic. The ceramide with 8-carbon hydrocarbon tails was found to adopt a "surface-bound" configuration. In contrast, ceramide with 12- or 16-carbon tails was found to adopt "micelle-inserted" configuration. The effect of lipid environment was found to be the least on the oligosaccharide linked to the ceramide with hexadecyl tails. Thus, the headgroup conformation in this case is essentially the same as that of the free headgroup. This probably explains the lesser crypticity of glycolipids with longer hydrocarbon tails.

Introduction

Gangliosides are glycolipids with a complex carbohydrate headgroup. Neuronal membranes of the central nervous system contain the highest amount of gangliosides in the body. Due to their structural diversity and predominant localization on the plasma membrane, gangliosides have been implicated in various cell recognition[1] and signaling phenomena,[2,3] cell growth and differentiation,[4] and tumor progression.[5,6] Gangliosides have been identified to be important components of receptor complexes capable of modulating signals across the membrane.[1] Changes in ganglioside composition have been observed during both normal[2] and tumor cell[7] differentiation. The ability of gangliosides to act as cell surface receptors is exploited by certain bacteria for initial recognition and infection of the host cell.[8] Toxins secreted by *Clostridium botulinum*, *Clostridium tetani*, *Campylobacter jejuni*, *Vibrio cholerae*, *Escherichia coli*, and *Bordetella pertussis* are all known to have gangliosides as the natural ligands.[9]

The ganglioside−protein interactions at the cell surface are influenced, inter alia, by the conformation and flexibility of the exposed oligosaccharide headgroups. X-ray crystallographic studies of cerebrosides[10−12] and NMR spectroscopic studies of glucosylceramide[13] and glucosylglyceride[14] revealed different orientations for the saccharide headgroups. Molecular mechanics calculations have been carried out on glucosylcerebroside[15] and globosides.[16] These studies indicated that orientation of the saccharide headgroup is primarily determined by conformation of the linkage between the saccharide headgroup and ceramide moiety and several conformations were found to be favored for this linkage. On the basis of these results, it was suggested that different saccharide orientations exposing/masking different epitopes might explain variations in receptor specificities i.e., crypticity of glycolipids.[1,16]

Ganglioside GM1 (Gal5-β1→3-GalNAc4-β1→4-[Neu5Ac3-α2→3-]-Gal2-β1→4-Glc1-β1→1-Cer) present on the intestinal brush border membranes acts as the natural receptor for cholera toxin (CT).[9] CT can bind to GM1 even when the lipid portion anchoring GM1 is replaced by proteins, but cannot elicit any intracellular response.[17] Binding of CT to the pentasaccharide portion alone is much weaker and replacement of the lipid portion of GM1 by acetyl group showed more effective binding to the toxin.[18] Thus, it was suggested that the lipid portion of GM1 per se is not necessary for toxin binding but it has some as yet unknown function.[18,19] Recent studies have shown that bilayer and the nature of the aglycon anchoring gangliosides *do indeed* influence ganglioside−protein interactions.[1]

NMR spectroscopic studies of GM3 (Neu5Ac3-α2→3-Gal2-β1→4-Glc1-β1→1-Cer) anchored in dodecylphosphocholine (DPC)/D_2O micelles (1:40 molar ratio) found the flexibility of Neu5Ac3-α2→3-Gal2 linkage and the mobility of GM3 in the micelles to be similar to that of GM3 in Me_2SO.[20] Multinuclear

* Author to whom correspondence should be addressed. Tel.: +91-22-576-7778. Fax: +91-22-572-3480. E-mail: balaji@btc.iitb.ac.in.

10.1021/jp0027952 CCC: $20.00
Published on Web 06/20/2001

NMR spectroscopic studies on the headgroup dynamics of GD1a (Neu5Ac-α2→3-Gal5-β1→3-GalNAc4-β1→4-[Neu5Ac-α2→3-]-Gal2-β1→4-Glc1-β1→1-Cer) at DPC micellar surface found evidence for conformational averaging.[21] Only the (180,−120) conformation was observed for the Neu5Ac-α2→3-linked to Gal2 whereas both (180,−120) and (−60,−120) were found for Neu5Ac-α2→3-linked to Gal5. The Gal5-β1→3-GalNAc4 linkage was found to sample several conformations with (ϕ,ψ) values around (−80,−90), (−80,−150), and (−150,−150). This study, however, could not determine if the headgroup orientation is unique or if it adopts multiple conformations. Using wide-line ^{2}H NMR, Grant and co-workers tested the effect of hydrocarbon chain variability, temperature, presence of cholesterol and charged residue in the headgroup on the behavior of glycosphingolipid headgroups in model membrane.[22] Partially deuterated GM1, asialo-GM1, and globoside were studied as examples in 1-palmitoyl-2-oleoylphosphatidylcholine bilayers. This study found only modest influence of the various factors tested on the preferred average conformation of the oligosaccharide.

Micelles have been widely used in various experimental studies to address membrane-related issues.[23−28] The present study aims at investigating, in atomic detail, the effect of lipid environment and the length of the hydrocarbon chain on the flexibility and conformation of the ganglioside headgroup. Molecular dynamics (MD) simulations have been performed for 1 ns on GM1 embedded-DPC micelle in water to investigate the possible in vivo conformations adopted by the ganglioside. Independent simulations were run for models wherein ceramide had octyl, dodecyl, and hexadecyl hydrocarbon chains to determine the effect of ceramide tail length on the headgroup dynamics and orientation. Simulations have also been performed on the free ganglioside headgroup (GM1-Os) in water and have been compared with that of GM1 embedded in micelle. Based on these studies, an attempt has been made to provide a stereochemical explanation for the observed crypticity of glycolipids.

Methods

Conventions and Definitions. The residues of the oligosaccharide are numbered sequentially. The glycosidic linkages are given the same number as the reducing sugar of that linkage (Figure 1). The glycosidic linkage ϕ is defined as O5−C1−O−CX′ except in Neu5Ac3-α2→3-Gal2 where it is taken as C1−C2−O−C3′; angle ψ is defined as C1−O−CX′−C(X − 1)′. The angles ϕ1, ψ1, and θ1 around Glc1-β1→1-Cer are defined as O5−C1−O1−C1(Cer), C1−O1−C1(Cer)−C2(Cer), and O1−C1(Cer)−C2(Cer)−C3(Cer), respectively, (Figure 1).

Generation of the Micelle. The DPC micelle was generated using the Euler's rigid body rotation method.[29] First, a molecule of DPC (23 atoms) was oriented such that the terminal methyl group is offset by 5 Å from the origin and the hydrocarbon tail is along the *X*-axis in the *XY*-plane. Using this as a template, fourteen DPC molecules were generated in the *XY*-plane by rotations around the *Z*-axis (25° increments from 10 to 340). In the next step, treating this set of 14 DPC molecules as a rigid body, rotations were performed around the *X*-axis (25° increments from 0 to 150°) that resulted in a micelle of 98 monomers. From this, 12 monomers were deleted by visual inspection to reduce crowding along both positive and negative *X*-directions. The resulting micelle with 86 monomers was considered as the starting configuration for 400-steps of energy minimization.

Generation of GM1-Os and GM1-Inserted Micelle. Coordinates for GM1-Os and GM1 were generated based on the

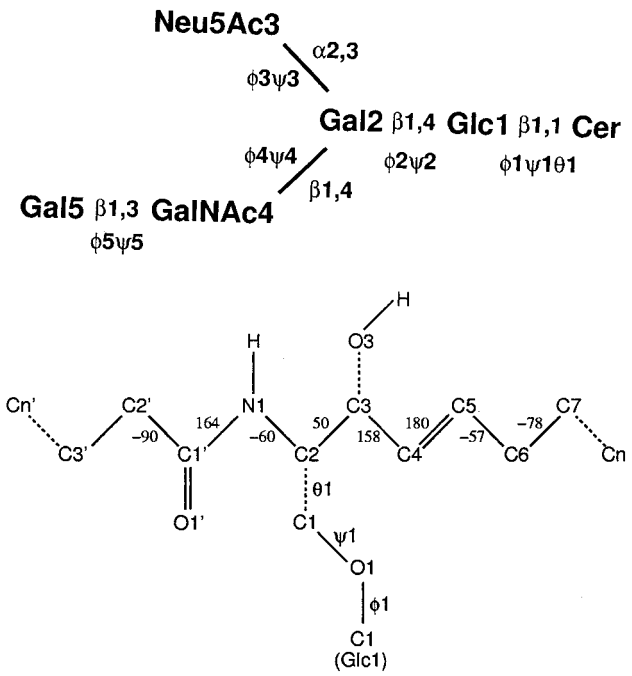

Figure 1. Schematic showing residue and torsion angle numbering for the oligosaccharide headgroup of GM1 (top) and atom nomenclature for ceramide (bottom). Initial conformations around the C−C bonds of the ceramide chain are trans except as indicated and are from ref 10.

X-ray crystallographic study of cerebroside[10] and standard geometry. Two DPC monomers in the energy minimized DPC micelle were replaced by a molecule of ganglioside GM1. The replacement was done such that GM1 is in a micelle-inserted orientation with its hydrocarbon tails embedded in the micelle and sugar headgroup facing the aqueous layer. The replacement did not result in any steric clashes between GM1 and other DPC monomers.

In the models with octyl and dodecyl chains, the oligosaccharide headgroup is on par with the phosphocholine headgroups of DPC. In the former case the hydrocarbon chain do not penetrate all the way into the center of the micelle because of shorter chain length. In the model with hexadecyl chains, the headgroup is offset from the surface of the micelle due to the presence of four additional carbon atoms in ceramide compared to DPC.

The aggregation number of a micelle has been shown to be influenced by temperature, nature and length of the hydrocarbon chain, nature of the headgroup, salt concentration, and other associated molecules.[23,30−32] It has also been suggested that micelles do not have one definite size but comprise a large range of aggregation numbers with a concentration maximum around a mean aggregation number.[30] Unfortunately, the aggregation number is not known for a DPC micelle which has a ganglioside accommodated in it. Although the aggregation number for pure DPC micelles has been found to be 56 ± 5 at 20 °C,[31] for dodecyl detergent micelles in general, the aggregation number has been observed to range from 50 to 90 at 25 °C.[30] Hence, the micelle model with 84 DPC monomers and a molecule of GM1 as has been used in the present study seems to be reasonable to determine the possible conformations of GM1 in a membrane environment.

Initial Conformations. The oligosaccharide moiety of GM1 was initially modeled to project away from the micelle surface. The headgroup conformation was based on MD simulations and is the same in both the simulations: (ϕ2,ψ2) = (−60,90); (ϕ3,ψ3) = (−70,−110); (ϕ4,ψ4) = (−60,−120); and (ϕ5,ψ5)

TABLE 1: Simulations of GM1 Embedded in DPC Micelle

simulation	length of ceramide tails	(θ1 ,ψ1)	number of water molecules	box size (nm)
I	12	(60,94)	10 638	7.00 × 9.00 × 6.00
II	12	(−150,−135)	8 185	8.20 × 6.08 × 6.05
III	8	(60,94)	6 824	6.18 × 7.00 × 6.00
IV	16	(60,94)	8 489	6.29 × 8.00 × 6.18

= (−60,−120). The conformations for the exocyclic hydroxyl groups were chosen randomly. The conformation of the ceramide chain is as indicated in Figure 1. The final system configuration had, besides GM1 and 84 DPC monomers, water molecules in a rectangular box. See Summary in Table 1. Five simulations, A to E, were run for GM1-Os. The initial conformations were chosen on the basis of in vacuo energy minimization of 20 different conformations of GM1-Os (data not shown). The number of water molecules and the size of the simulation box are shown in Table 2.

Software and Force Field. All simulations were done using molecular simulation package GROMACS2.0[33,34] on Origin 200-compute servers. RASMOL was used for visualization.[35] In-house programs were used for analysis and these will be available upon request. The building blocks for DPC, ceramide, and various monosaccharides were generated using in-house programs since they are not available in the standard GROMACS residue library. These building blocks are also available from the authors upon request. The GROMOS96 force field was used for all the calculations[36] except for the fractional atomic charges for the phosphocholine moiety, which are from Chiu et al.[37] The GROMOS96 force field uses united atom approach for CH, CH_2, and CH_3 groups and it does not have an explicit hydrogen bonding term. The steepest descent algorithm was chosen for energy minimization.

Simulations. The energy-minimized system (GM1-Os or GM1 in DPC micelle) was placed in the center of a rectangular box of SPC water corresponding to a density of 1.03 g/cm^3. The solvated system was energy minimized without constraints for 500 steps to remove close contacts of water molecules with solute. This was followed by a 1 ps MD equilibration run by positionally restraining the solute atoms to relax the water molecules. The solute restraints were removed for the subsequent 200 ps equilibration run. The productive runs were for 1 ns duration, and the trajectories were saved at 1 ps interval. Only data from the productive run were used for analysis.

The equations of motion were integrated using Verlet's leapfrog algorithm with a 2 fs time step. Initial velocities were assigned from Maxwellian distribution using a random number generator corresponding to a temperature of 300 K. Temperature was maintained constant by coupling the solute and solvent separately to a 300 K temperature bath with a relaxation time of 0.1 ps. No pressure coupling was used. Periodic boundary conditions were applied and nonbonded interactions were calculated using a neighbor list cut-off of 1.5 nm. The nonbonded atom list was updated after every 50 steps. The dielectric constant was set to 80. All bond lengths were constrained using linear constraint solver.[38]

Results and Discussion

Conformation of Free Oligosaccharide Headgroup, GM1-Os. *β1→4-linkages.* The Gal2-β1→4-Glc1 linkage accesses all the allowed regions[39] and has complete conformational freedom as in an independent disaccharide. Thus, the conformation of Gal2-β1→4-Glc1 in GM1-Os is independent of other residues of the oligosaccharide. The angle ϕ2 shows transitions between the *-sc* and *-ap* regions (Figure 2A). The *+sc* region is also accessed, but for short periods of time (∼40 to 275 ps in different simulations). The angle ψ2 oscillates between *+sc*/*+ac* and *+ap* regions but the latter is excluded when ϕ2 is in the *-ap* region. Transitions between different allowed regions are observed during the simulations. Conformations similar to those observed in these simulations have also been deduced from NMR and potential energy calculations for asialo-GM1,[40] asialo-GM2, and related synthetic haptens,[41] GD1a-Os,[42] and GM3-Os.[43] Acquotti et al.[44] found that any of the four conformations (−65,120), (−85,70), (−115,90), and (−90,50) is able to satisfactorily model the observed NOEs in GM1.

The β1→4-linkage between GalNAc4 and Gal2 is at the branch point of GM1-Os. For this linkage, ϕ4 prefers the *-sc*/*-ac* region in all the simulations (Figure 2B). In simulation D, where ϕ4 is initially in the *+sc* region, transition to the *-ac* region occurs at ∼360 ps. Transitions from the *-ac* region to the *-ap* region are seen but for only durations of ∼30 to 100 ps. ψ4 shows frequent transitions between *-sc* and *-ap/anti* regions. These values of (ϕ4,ψ4) are in good agreement with those derived from the molecular mechanics calculations and MD simulations combined with NMR spectroscopic data of asialo-GM1-Os,[40,41] GD1a-Os,[42] GM1-Os,[44] and GalNAc-GD1a-Os.[45] Even though the conformational regions allowed for all the β1→X linkages are essentially the same,[39] the GalNAc4-β1→4-Gal2 has reduced conformational freedom compared to Gal2-β1→4-Glc1. This is primarily due to the axial orientation of the O−4′ glycosidic bond.

β1→3-linkage. The terminal Gal5-β1→3-GalNAc4 prefers conformations in both *-sc*/*-ac* and *-ap* regions of ϕ5 and ψ5; the *-sc* region being accessed for longer durations for both angles and transitions are frequently observed from one region to another. However, the conformations of ψ5 are correlated to those of ϕ5: when ϕ5 is in the *-ap* region, ψ5 is also excluded from the *-sc* region (Figure 2C). In simulations where ϕ5 is initially in the *+sc* region, a higher energy local minimum,[46] transitions to the preferred *-sc* region occur during equilibration. The regions of the conformational map accessed by Gal-β1→3-GalNAc moiety are same as those found in other gangliosides.[40−45] The similarity of the conformational preferences with β1→3-linked disaccharides[47−49] implies that other constituent linkages of GM1-Os do not influence the conformation of this moiety.

α2→3-linkage. In Neu5Ac3-α2→3-Gal2, ϕ3 is observed to prefer the *-sc* region but transitions to the *-ap* and *+sc* regions are also observed (Figure 2D). In simulation A, where the initial conformation of ϕ3 is *+sc*, transition is observed to *-sc* region during the 200 ps equilibration run. In all the simulations A to E, the angle ψ3 is observed to remain in *-ac*/*-ap* regions (Figure 2D). Energy minimization studies of Neu5Ac-α2→3-Gal with rigid pyranose rings found ψ to be around −130 and ϕ to prefer all the three staggered conformations, anti being a higher energy minimum.[39,50,51] Solution conformation of this disaccharide has also been investigated with the aid of ^{1}H NMR spectroscopy in conjunction with MM2 force-field-based energy minimization studies.[52] The latter studies gave three conformers **1**, **2,** and **3** with (ϕ,ψ) = (−153,−94), (−85,−108), and (61,−134). 1D steady-state NOE measurements indicated that the disaccharide exists as a mixture of only conformers **1** and **2**; the third conformer could not be detected. Further, NOE data were able to provide the occupancy factor for only conformer 1 (about 40%). The ∼60% occupancy left for conformer **2** could not be independently confirmed by these NMR studies. Empirical potential energy calculations also identified a conformation close

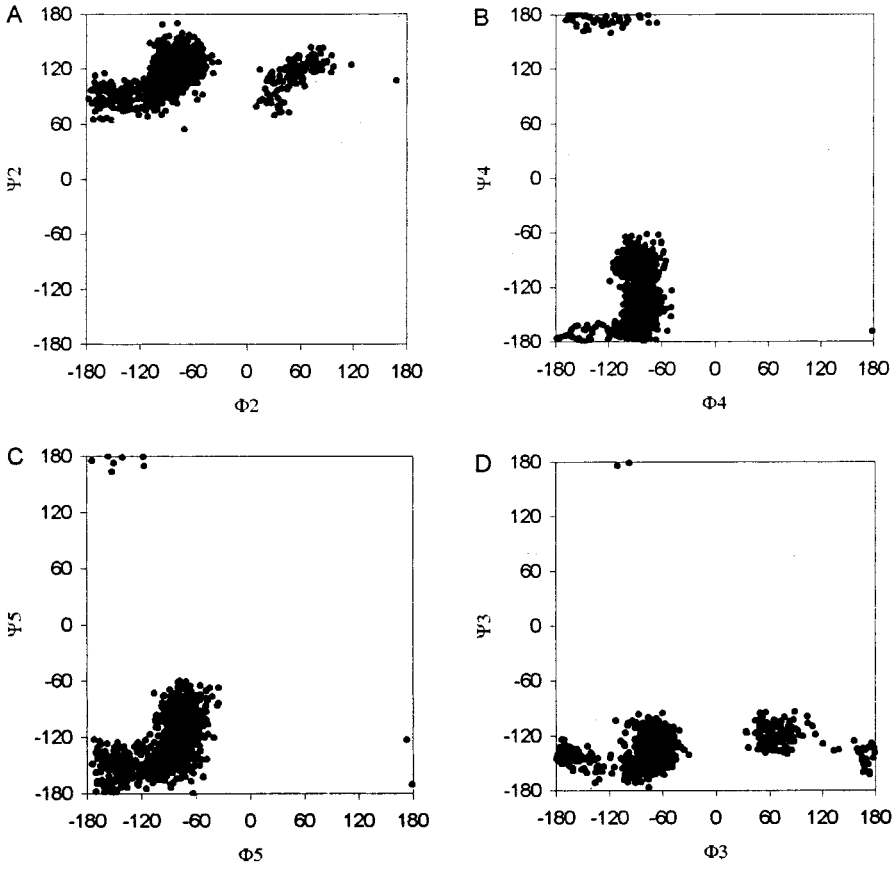

Figure 2. Plots of (ϕ,ψ) from the simulations of GM1-Os. (A; *top left*) Plot of (ϕ2,ψ2) from simulation A. In Glc1-β1→4-Gal2, ϕ2 and ψ2 are correlated; when ϕ2 is in the *-ap* region, +*ap* region is excluded for ψ2. (B; *top right*) Plot of (ϕ4,ι4) from simulation B. This occurs at the branching point of GM1. ϕ4 prefers the *-sc*/*-ac* region in all the simulations. Transitions from the *-ac* region to the *-ap* region are seen for only short durations. ψ4 shows frequent transitions between *-sc* and *-ap* regions. (C; *bottom left*) Plot of (ϕ5,ψ5) from simulation A. This pair of glycosidic angles decides the conformation of terminal Gal5. This terminal linkage is observed to be more flexible as compared to the terminal α-2→3-linked sialic acid in GM1-Os. (D; *bottom right*) Plot of (ϕ3,ψ3) from simulation D. In all the five simulations, ϕ3 prefers the *-sc* region but transitions to *-ap* and +*sc* regions are observed. Angle ψ3 is observed to remain at *-ac*/*-ap* region. In simulation A, where the initial conformation of ϕ3 is +*sc*, transition is observed to *-sc* region during the 200 ps equilibration run.

TABLE 2: GM1-Os Simulations

simulation	initial values (ϕ2,ψ2)	(ϕ3,ψ3)	(ϕ4,ψ4)	(ϕ5,ψ5)	number of water molecules	box size (nm)
A	(45,126)	(55,−113)	(−73,−101)	(−41,−142)	1198	3.40 × 3.25 × 3.32
B	(47,125)	(−60,−143)	(−72,−106)	(52,−110)	1213	3.13 × 3.51 × 3.34
C	(−66,127)	(−58,−144)	(−66,−111	(50,−106)	1086	3.00 × 3.26 × 3.45
D	(50,120)	(−170,−116)	(31,−109)	(61,−120)	1019	2.98 × 3.33 × 3.25
E	(50,120)	(−70,−118)	(−70,−114)	(47,−106)	1203	3.15 × 3.42 × 3.38

to conformer **2** as the preferred conformation.[53] X-ray crystallographic studies of sialyllactose (Neu5Ac-α2→3-Gal-β1→4-Glc) bound to sialoadhesin,[54] to influenza virus haemagglutinin[55,56] and to wheat germ agglutinin[57] showed the Neu5Ac-α2→3-Gal fragment to be in the (−70,−136), (−60,−120), (−60,−132), and (−62,−125) conformations, respectively. In the crystal structure of cholera toxin complexed with GM1-Os, ϕ3 is in the anti conformation.[58] NMR and HSEA calculation of GD1a-Os,[42] GalNAc-GD1a-Os,[45] and GM1-Os[44] also found the anti conformation for ϕ3. Thus, the MD simulations show the individual glycosidic linkages of GM1-Os to be essentially as flexible as the corresponding disaccharides.

Structure and Dynamics of the GM1-Embedded Micelle. About 10 to 15% of the C−C bonds of DPC are in gauche conformation (Figure 3A) and no positional preference was found for the location of these gauche bonds in the hydrocarbon tails (data not shown). The terminal methyl carbon atom (C12) is found at various distances from the center of mass and some of the hydrocarbon tails were found on the micelle surface also (Figure 3B). However, the N atom of the choline moiety has a comparatively narrow distribution. The choline headgroup is more solvated compared to the phosphate oxygen atoms (Figure 3C). Penetration of water molecules into the interior of the micelle was also observed (Figure 3D). The structure and dynamics of the DPC micelle as found in this study are very similar to that reported earlier based on the MD simulations of pure DPC micelles (i.e., without any associated protein or carbohydrate moieties) using CHARMM[59] and GROMACS[60] force fields. The micelle structure also complies with the lattice model proposed by Dill and Flory[61] for amphiphilic aggregates.

Conformation of Oligosaccharide Headgroup in Micelle-Anchored GM1. The Gal2-β1→4-Glc1 linkage was found to be very flexible in GM1-Os; however, when GM1-Os is anchored in the micelle, ϕ2 shows preference for the *-sc* region with ψ2 occupying the anti region (Figure 4A). The +*sc* and anti regions are not accessed by ϕ2 in any of the simulations I

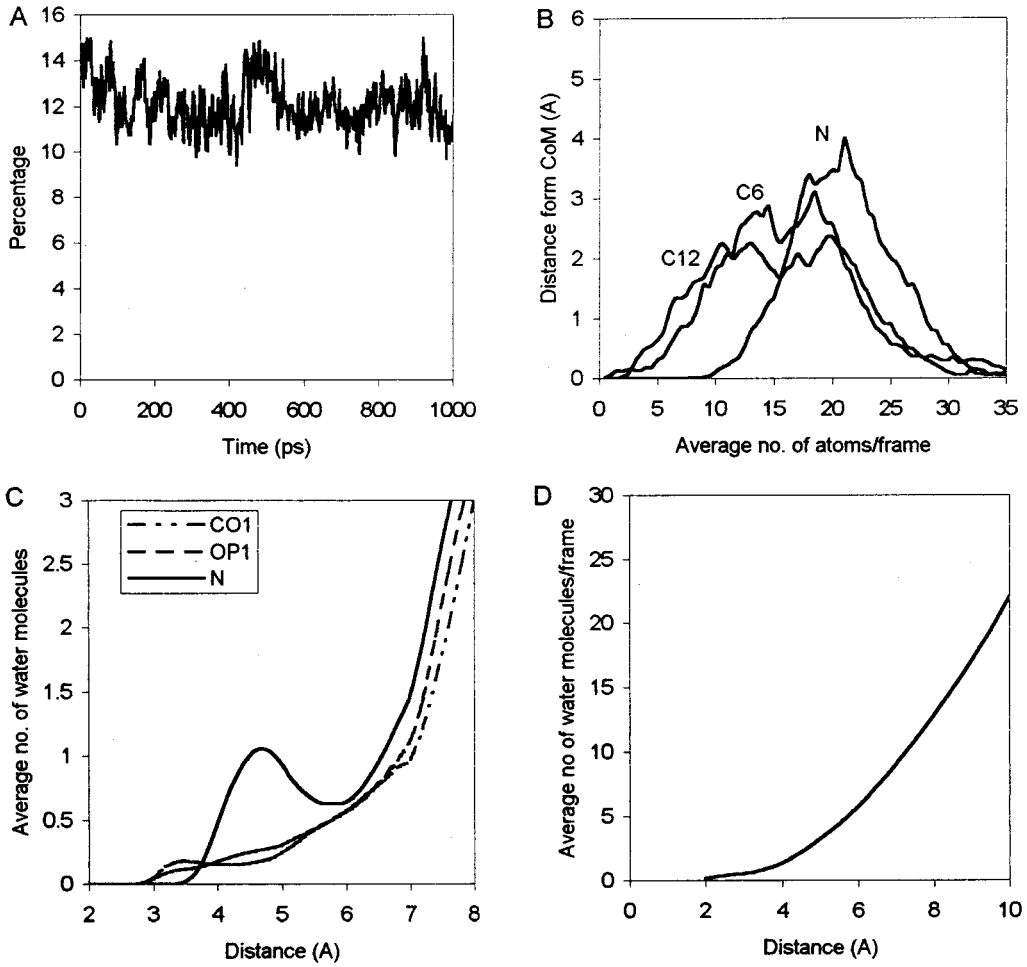

Figure 3. Structure and dynamics of DPC micelle. **(**A; *top left*) Variation of the percentage of C−C bonds found in gauche conformation (i.e., |dihedral angle| < 100) during the 1 ns productive run. For each frame, the average was calculated over the 9 C−C bonds for each of the 84 DPC monomers. The profiles for the individual C−C bonds look essentially the same indicating the absence of positional preference for the gauche conformation. (B; *top right*) The average number of C12, C6 and N atoms (84 atoms per micelle in each of the 1000 frames) found within spherical shells of increasing radius (0.5 Å intervals) from the center of mass. (C; *bottom left*) Average number of water molecules around phosphocholine headgroup atoms CO1, OP1 and N. The distribution of O1 is very similar to that of CO1. Intervals of 0.2 Å were considered for the *X*-axis. The average is calculated for 84 000 atoms (84 atoms per micelle in each of the 1000 frames) (D; *bottom right*) Average number of water molecules found within spherical shells of increasing radii (2 Å intervals) from the center of mass. The average is calculated by counting the number of water molecules within respective distance intervals in all the 1000 frames.

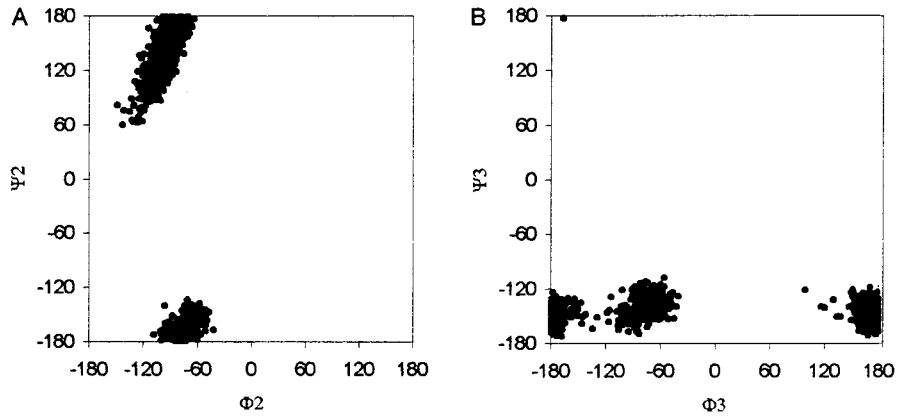

Figure 4. Plots of (ϕ,ψ) from the simulation of GM1 embedded in micelle. (A; *left*) Plot of (ϕ2,ψ2) from simulation II. The Glc1-β1→4-Gal2 linkage is restricted when GM1 is embedded in micelle; ϕ2 shows preference for the *-sc* region with ψ2 occupying the anti region. (B; *right*) Plot of (ϕ3,ψ3) from simulation IV. The transition from the *-sc* to the anti region is seen only for GM1 with hexadecyl ceramide tails.

to IV. However, in simulation I, (ϕ2,ψ2) shows transition to the (*-ap*,*+sc*) region after ∼550 ps and in simulation III, it accesses this region for ∼80 ps (549 to 628 ps). The α2→3-linkage is found to be restricted to the (*-sc*,*-ap*) region with an average value of (ϕ3,ψ3) = (−67,−130) (standard deviation of 12 for ϕ3 and 11 for ψ3) except in GM1 with hexadecyl ceramide tails (i.e., simulation IV) where it shows transitions to the (*ap*,*-ap*) region (Figure 4B). The transitions of ϕ3 from the *-sc* to the *+sc* and *-ap* regions seen for GM1-Os are not observed when GM1 is anchored in the micelle. Thus, the

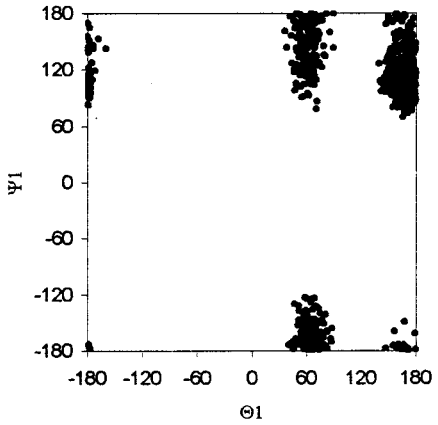

Figure 5. Plot of $\theta 1$ versus $\psi 1$ from simulation IV. Angle $\psi 1$ prefers a wider region from $+ac$ to $-ac$ and shows similar variations in all the four simulations i.e., I to IV. However, $\theta 1$ accesses different staggered conformations in different simulations: it is in the $+sc$ region in simulation I and in the $-sc$ region in simulations II and III. Average values for ($\theta 1$,$\psi 1$) are (67,154) (standard deviation (11,37)) in simulation I, (−63,−163) (standard deviation (8,24)) in simulation II, and (−63,160) (standard deviation (9,43)) in simulation III.

flexibility of the sialic acid moiety is comparable to that in GM1-Os only when GM1 has a longer ceramide tail. The terminal Gal5-β1→3-GalNAc4 linkage behaves similar to that in GM1-Os in all simulations (data not shown). However, for the GalNAc4-β1→4-Gal2 linkage, the (*-ap*,*-ap*) region accessed for short durations in GM1-Os is not at all accessed in any of the simulations I to IV. In addition, the (*-sc*,anti) region is also not accessed when GM1 has shorter hydrocarbon tail (i.e., in simulation III); ($\phi 4$,$\psi 4$) is restricted to the (*-sc*,*-ap*) region with an average value of (−80,−136) (standard deviation of 11 for $\phi 4$ and 24 for $\psi 4$). The restrictions observed on the conformations of ($\phi 4$,$\psi 4$) are particularly noteworthy since the GalNAc4-β1→4-Gal2 is a branch point; changes in the conformation of this linkage affect the orientation and/or accessibility of all the residues linked beyond this point.

Conformation of Ceramide−Saccharide Linkage. The angles ($\phi 1$,$\psi 1$,$\theta 1$) (Figure 1) define the conformation of ceramide−saccharide linkage. In simulations I, III, and IV, $\phi 1$ is in the *-sc* region whereas in simulation II, it prefers the $+sc$ region. X-ray crystallographic[10−12] and molecular modeling studies[16] found $\phi 1$ to prefer the *-sc* region in glycosylceramides. The sterically allowed regions for $\psi 1$ and $\theta 1$ were found to be dependent on the length of the ceramide hydrocarbon tails and the extent to which the ceramide is buried: the allowed region for ($\theta 1$,$\psi 1$) in GM1 with hexadecyl hydrocarbon tails is more than that in GM1 having shorter hydrocarbon chains (data not shown). The angle $\psi 1$ accesses a wider range of conformational area from $+ac$ to $-ac$ in all the four simulations; however, $\theta 1$ prefers different staggered conformations in different simulations (Figure 5). Previously, MM3 calculations on β-D-glucosylceramide have been carried out by considering an exclusion plane at the level of C1(Cer) to account for the restrictions imposed by membrane; from this, it was concluded that $\psi 1$ accesses all the three staggered conformations when $\theta 1$ is anti and vice versa.[15]

Ceramide Dynamics. The C−C bonds in the hydrocarbon tails of GM1, except as noted below, essentially remain all-trans but show frequent transitions to the $\pm sc$ regions suggesting that, like DPC monomers, the ceramide tails are also dynamic. These transitions are probably coordinated with those of the DPC hydrocarbon tail for efficient packing of the micelle interior. The C6−C7 bond, initially in the *-sc* region, is mostly

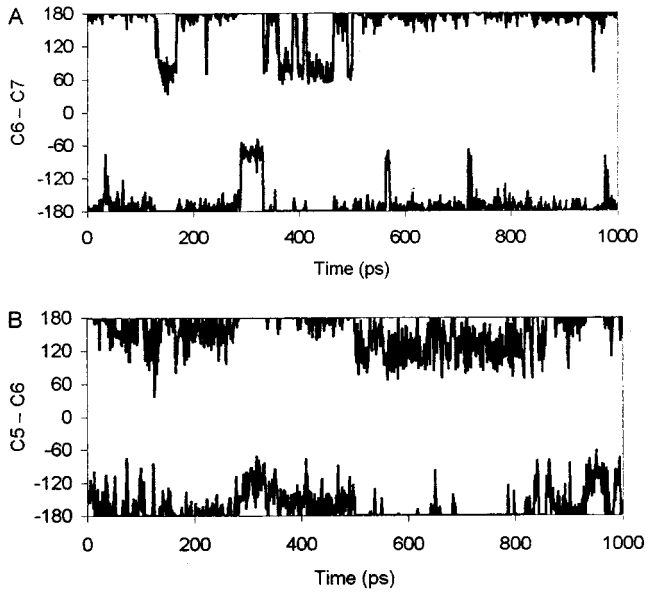

Figure 6. (A; top) Plot of conformation found around C6−C7 versus time from simulation I. The C6−C7 bond, initially in the *-sc* region, is mostly in the *anti* region. (B; bottom) Plot of conformation around C5−C6 as a function of time from simulation I. C5−C6 bond is observed to be flexible and it accesses conformational space from $+ac$ to $-ac$ regions. In this and Figure 7, time 0 refers to the first frame after 200 ps of equilibration run, i.e., the beginning of the productive run.

restricted to the anti region but shows transitions to the $\pm sc$ regions for short intervals of time (∼50 to 80 ps) (Figure 6A). In contrast, the C5−C6 bond shows much more flexibility accessing a very large conformational space from $-ac$ to $+ac$ (Figure 6B). A change in the conformation of N1−C2 bond from the initial $-sc$ to the $+sc$ region with a concomitant trans to cis change in the amide bond is seen in simulations I and IV. The intramolecular hydrogen bond H(N1)→O1(Glc1), observed in cerebroside crystals,[10] was found in simulations II and III for about 56 to 72% of the total simulation time. In the other two simulations, this hydrogen bond is absent due to the absence of −90 and −60 conformations around the N1−C2 and C2−C1 bonds, respectively.

The hydrocarbon tails of ceramide are initially micelle-inserted in all the four simulations (I to IV). The initial headgroup position is on par with the micelle surface in simulations I, II, and III; however, it is offset from the surface due to longer tail length (i.e., 16 carbons) in simulation IV. The configuration of the ceramide tails during the simulation was deduced on the basis of the distance of the terminal methyl carbon atoms from the center of mass. In simulations I and II, wherein ceramide has dodecyl hydrocarbon chains, one of the tails is micelle-inserted and the other is surface-bound (Figure 7A). As a consequence, the distance between the two terminal methyl groups, initially ∼5 Å, increases to >15 Å (data not shown). In simulation III, both the octyl hydrocarbon tails of the ceramide are surface-bound suggesting that the hydrocarbon tail is too short to have a micelle-inserted configuration (Figure 7B). The transition from the initial micelle-inserted to the surface-bound configuration in simulation III is smooth and occurs at about 500 ps of the productive run. The persistence of this configuration for the rest of the simulation suggests that glycolipids with shorter ceramide tails probably prefer a surface-bound configuration. In simulation IV, wherein the ceramide has long hexadecyl tails, both are micelle-inserted and remain essentially parallel to each other (Figure 7C).

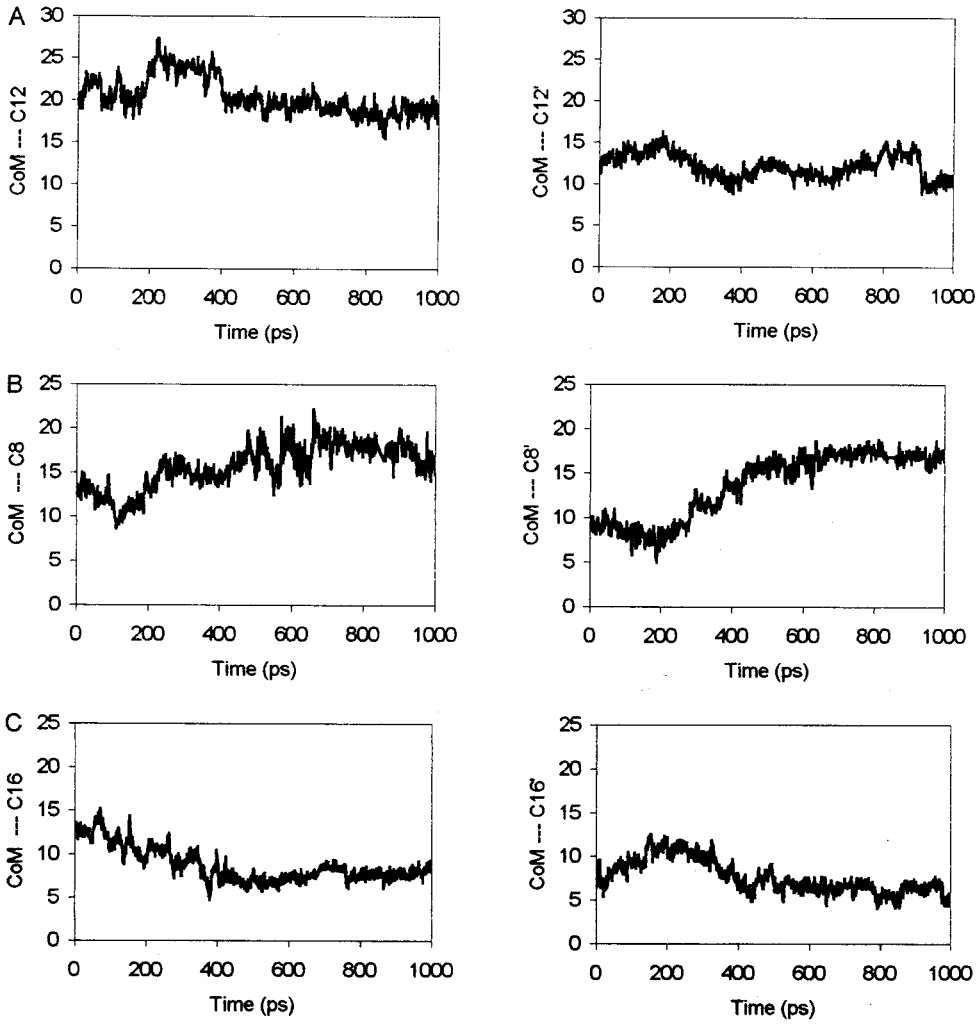

Figure 7. Plots to show the position of the terminal methyl group of ceramide tails relative to the center of mass of micelle. The distance (in Å) of the respective atom has been plotted as a function of time (Refer to Figure 1 for atom nomenclature). The tail is inferred to be micelle-inserted if the distance is small whereas larger distances have been taken to imply surface-bound configuration. (A; *top*) Simulation I: One of the dodecyl tails is micelle-inserted whereas the other is surface-bound. (B; *middle*) Simulation III: Both the octyl hydrocarbon tails are surface-bound. (C; *bottom*) Simulation IV: Both the hexadecyl hydrocarbon tails are micelle-inserted.

Orientation of Oligosaccharide Headgroup Relative to the Micelle. Molecular modeling of micelle-anchored GM1 showed that, angle ϕ1, unlike θ1 and ψ1, has practically no effect on the orientation of the headgroup *relative* to the micelle surface. In other words, the effect of ϕ1 rotation is similar to the rotation of the headgroup around an axis perpendicular to the micelle surface. In simulation IV, where the hydrocarbon tails are 16-carbon long, and the headgroup is offset from the membrane surface, θ1 and ψ1 are observed to exhibit maximum flexibility (Figure 5) suggesting least influence from the micellar environment. The oligosaccharide headgroup lies on the micelle surface with a membrane-parallel orientation in all the simulations including simulation IV where the headgroup was initially projecting away from the surface. Despite the proximity of the oligosaccharide to the DPC monomers, very few hydrogen-bonding interactions are observed between them. This is mainly due to the continuous rotations of the hydroxyl hydrogen atoms (i.e., around C−O bonds) of the saccharide and the relatively buried hydrogen bond acceptors (i.e., phosphate oxygen atoms) of DPC.

Effect of Micellar Environment on Oligosaccharide Dynamics. It is noteworthy that the conformation of the oligosaccharide headgroup and its orientation relative to the micelle surface are intimately linked to the orientation of the ceramide hydrocarbon tails and the conformation of the ceramide bonds close to the point of oligosaccharide attachment. These, in turn, are influenced by the packing considerations of the micelle as a whole. GM1 with short ceramide hydrocarbon tails (i.e., 8-carbon long) is almost in a surface-bound configuration. When GM1 has longer ceramide tails (i.e., 16-carbon long), even though hydrocarbons are inserted into the micelle, its conformation is independent of the micelle dynamics. However, the (*-ap*,*-ap*) region for GalNAc-β1→4-Gal, accessed for a short duration by GM1-Os, is disallowed in the micellar environment (Figures 2 and 4). In addition, when ϕ4 is in the *-ac* region, ψ4 is restricted to the *-ac* region and the *-ap* region is disallowed in simulation III. This linkage, being a branch point, affects the orientation/accessibility of all the residues linked to GalNAc.

Oligosaccharide Crypticity. Crypticity has been described as a phenomenon whereby cell surface receptors, although present, are inaccessible to/not recognized by their specific macromolecular ligands.[1] Modulation of receptor recognition/binding by structural changes not associated with the recognized moiety per se has previously been reported.[18,19,62] It has been suggested that crypticity can be induced by the lateral distribution, motional properties, orientation and degree of protrusion of the oligosaccharide from the membrane surface.[22] In addition, the fatty acid composition of glycosphingolipids and the lipid

nature of the host membrane have also been suggested to influence the crypticity.[1,22] Earlier NMR observations concluded that the oligosaccharide headgroups in lipid environment have the same average conformation as the free oligosaccharides.[20−22] The results of the present MD simulation show that, certain conformational regions are either restricted or are completely excluded for the β1→4-arm and to some extent, for the Neu5Ac-α2→3 linkage. It has to be noted that the protein-bound conformations are not necessarily the predominant solution conformations;[63−66] besides, different proteins bind to ligands in different conformations—for example, α2→3-linked Neu5Ac bound to cholera toxin is in the anti conformation[58] whereas it is in the *-sc* region when bound to sialoadhesin,[54] influenza virus haemagglutinin,[55,56] and wheat germ agglutinin.[57] Thus crypticity of the oligosaccharide is probably due to the unavailability of the required conformation of the oligosaccharide for binding to ligand. The observation that the effect of micellar environment is least on GM1 with hexadecyl ceramide tails is in consonance with the observation that longer glycolipids are less cryptic.

Conclusions

This work reports 1 ns MD simulation studies on the behavior of GM1 in a DPC micellar environment and the comparison of headgroup conformation with that of GM1-Os. GM1-Os is very flexible and the conformational regions accessed by the individual glycosidic linkages are in good agreement with those reported earlier for similar linkages. The conformations of the headgroup, ceramide-saccharide linkage and hydrocarbon tails were found to be inter-related and are, in turn, influenced by micellar packing considerations. The conformations of GalNAc-β1→4-Gal and Neu5Ac-α2→3-Gal linkages were found to be restricted when GM1 is embedded in the micellar compared to that in GM1-Os. This elimination of certain conformational regions is found to be dependent on the conformation around ceramide-saccharide linkage and length of the hydrocarbon tails. This could lead to crypticity as specific binding to cell surface receptors is governed by recognition of specific conformations of these receptors by the ligands.

Acknowledgment. We thank Prof. Y. U. Sasidhar, Department of Chemistry, for helpful discussions and critical reading of the manuscript. We also thank the Computer Centre, IIT, Bombay for allocation of computing time and staff support. The authors are especially thankful to Dr. J. Maharana, Computer Center, for his help in resource management. S.V.V. is grateful to the Indian Institute of Technology, Bombay, for a teaching assistantship. This research was supported by a grant (SP/SO/D-07/96) from the Department of Science and Technology, India to P.V.B.

References and Notes

(1) Evans, S. V.; MacKenzie, C. R. *J. Mol. Recognit*. **1999**, *12*, 155.
(2) Fishman, P. H.; Pacuszka, T.; Oralandi, P. A. *Adv. Lipid Res*. **1993**, *25*, 165.
(3) Schengrund, C.-L. *Biol. Signals* **1995**, *4*, 1.
(4) Nohara, K.; Kunimoto, M.; Fujimaki, H. *J. Biochem.* **1998**, *124*, 194.
(5) Ladisch, S.; Chang, F.; Li, R.; Cogen, P.; Johnson, D. *Cancer Lett*. **1997**, *120*, 71.
(6) Yohe, H. C.; Ye, S.; Reinhold: B. B.; Reinhold: V. N. *Glycobiology* **1997**, *7*, 1215.
(7) Simons, K.; Ikonen, E. *Nature* **1997**, *387*, 569.
(8) Sears, C. L.; Kaper, J. B. *Microbiol. Rev*. **1996**, *60*, 167.
(9) Merritt, E. A.; Hol, W. G. J. *Curr. Opin. Struct. Biol.* **1995**, *5*, 165.
(10) Pascher, I.; Sundell, S. *Chem. Phys. Lipids* **1977**, *20*, 175.
(11) Nyholm, P. G.; Pascher, I.; Sundell, S. *Chem. Phys. Lipids* **1990**, *52*, 1.
(12) Abrahamsson, S.; Dahlen, B.; Pascher, I. *Acta Crystallogr*. **1977**, *B33*, 2008.
(13) Skarjune, R.; Oldfield, E. *Biochemistry* **1982**, *21*, 3154.
(14) Jarell, H. C.; Jovall, P. A.; Giziewicz, J. B.; Turner, L. A.; Ian Smith, C. P. *Biochemistry* **1987**, *26*, 1805.
(15) Nyholm, P.-G.; Pascher, I. *Biochemistry* **1993**, *32*, 1225.
(16) Stromberg, N.; Nyholm, P. G.; Pascher, I.; Normark, S. *Proc. Natl. Acad. Sci. (U.S.A.)* **1991**, *88*, 9340.
(17) Pacuszka, T.; Fishman, P. H. *J. Biol. Chem*. **1990**, *265*, 7673.
(18) Fishman, P. H.; Pacuszka, T.; Hom, B.; Moss, J. *J. Biol. Chem.* **1980**, *255*, 7657.
(19) Schengrund, C.-L.; Ringler, N. J. *J. Biol. Chem*. **1989**, *264*, 13233.
(20) Siebert, H. -C.; Reuter, G.; Schauer, R.; von der Leith, C.-W.; Dabrowski, J. *Biochemistry* **1992**, *31*, 6962.
(21) Poppe, L.; Halbeek, H. van; Acquotti, D.; Sonnino, S. *Biophys. J*. **1994**, *66*, 1642.
(22) Singh. D. M.; Shan, X.; Davis, J. H.; Jones, D. H.; Grant, C. W. M. *Biochemistry* **1995**, *34*, 451.
(23) Beswick, V.; Guerois, R.; Cordier-Ochssenbein, F.; Coic, Y. M.; Tam, H. D.; Tostain, J.; Noel, J. P.; Sanson, A.; Neumann, J. M. *Eur. Biophys. J*. **1998**, *28*, 48.
(24) Kloosterman, D. A.; Goodwin, J. T.; Burton, P. S.; Conradi, R. A.; Stockman, B. J.; Scahill, T. A.; Blinn, J. R. *Biopolymers* **2000**, *53*, 396.
(25) Jarvet, J.; Zdunek, J.; Damberg, P.; Graslund, A. *Biochemistry* **1997**, *36*, 8153.
(26) Mercurio, E.; Pellegrini, M.; Mierke, D. F. *Biopolymers* **1997**, *42*, 759.
(27) Chorev, M.; Gurrath, M.; Behar, V.; Mammi, S.; Tonello, A.; Peggion, E. *Biopolymers* **1995**, *36*, 473.
(28) Wymore, T.; Wong, T. C. *Biophys. J*. **1999**, *76*, 1213.
(29) Goldstein, H. *Classical Mechanics*, 2nd ed.; Addison-Wesley Inc.: London, 1980; Chapter 5.
(30) Hoffmann, H.; Ulbricht, W. In *Thermodynamic data for biochemistry and biotechnology*; Springer-Verlag: Berlin, 1986; Chapter 12, p 298.
(31) Lauterwein, J.; Bosch, C.; Brown, L. R.; Wuthrich, K. *Biochim. Biophys. Acta* **1979**, *556*, 244.
(32) Jones, M. N.; Chapman, D. In *Micelles, monolayers and biomembranes*; Wiley-Liss: New York, 1995; Chapter 3, p 80.
(33) Berendson, H. J. C.; van der Spoel, D.; van Drunen, R. *Comput. Phys. Commun.* **1995**, *91*, 43.
(34) Van der Spoel, D.; van Buuren, A. R.; Apol, E.; Meulenhoff, P. J.; Tielman, D. P.; Sijbers, A. L. T. M.; Hess, B.; Feenstra, K. A.; Lindahl, E.; van Drunen, R.; Berendsen, H. J. C. *Gromacs User Manual version 2.0*; The Netherlands; http://md.chem.rug.nl/~gmx; 1999.
(35) Sayle, R. *RASMOL molecular visualisation program*; Biomolecular structures group, Glaxo Research and Development, Greenford, Middlesex, 1994.
(36) van Gunsteren, W. F.; Billeter, S. R.; Dusubg, A. A.; Hunenberger, P. H.; Kruger, P.; Mark, A. E.; Scott, W. R. P.; Tironi, I. G. *Biomolecular Simulation: The GROMOS96 manual and user guide*; Zurich, Switzerland: Hochschulverlag AG an der ETH Zurich, 1996.
(37) Chiu, S.-W.; Clark, M.; Balaji, V.; Subramaniam, S.; Scott, H. L.; Jakobosson, E. *Biophys. J*. **1995**, *69*, 1230.
(38) Hess, B.; Bekker, H.; Berendsen, H. J. C.; Fraaije, J. G. E. M. *J. Comput. Chem*. **1997**, *18*, 1463.
(39) Rao, V. S. R.; Qasba, P. K.; Balaji, P. V.; Chandrasekaran, R. *Conformation of Carbohydrates*; Harwood Academic: Singapore, 1998; Chapter 4.
(40) Park, H. J.; Han, S. J.; Kang, Y. K. *Biopolymers* **1997**, *42*, 19.
(41) Sabesan, S.; Bock, K.; Lemieux, R. U. *Can. J. Chem*. **1984**, *62*, 1034.
(42) Sabesan, S.; Duus, J.; Fukunaga, T.; Bock, K.; Ludvigsen, S. *J. Am. Chem. Soc*. **1991**, *113*, 3236.
(43) Siebert, H.; Reuter, G.; Schauer R.; von der Leith, C.-W.; Dabrowski, J. *Biochemistry* **1992**, *31*, 6962.
(44) Acquotti, D.; Poppe, L.; Darbrowski, J.; von der Lieth, C.-W.; Sonnino, S.; Tettamanti, G. *J. Am. Chem. Soc*. **1990**, *112*, 7772.
(45) Acquotti, D.; Cantu, L.; Ragg, E.; Sonnino, S. *Eur. J. Biochem.* **1994**, *225*, 271.
(46) Imberty, A.; Mikros, E.; Koca, J.; Mollicone, R.; Oriol, R.; Perez, S. *Glycoconj. J*. **1995**, *12*, 331.
(47) Yan, Z.-Y.; Bush, A. *Biopolymers* **1990**, *29*, 799.
(48) Kobayashi, H.; Kitamura, S.; Ozaki, T.; Yamaguchi, M.; Kuge, T. *Chem. Express* **1989**, *4*, 213.
(49) Yadav, J. S.; Luger, P. *Carbohydr. Res*. **1983**, *119*, 57.
(50) Veluraja, K. *Studies on the conformations of gangliosides*. Ph.D. Thesis, Indian Institute of Science, Bangalore; 1983.
(51) Veluraja, K.; Rao, V. S. R *Carbohydr. Polym.* **1983**, *4*, 357.
(52) Poppe, L.; Dabrowski, J.; von der Lieth, C.-W.; Numata, M.; Ogawa, T. *Eur. J. Biochem.* **1989**, *180*, 337.

(53) Wynn, C. H.; Marsden A.; Robson B. *J. Theor. Biol.* **1986**, *119*, 81.
(54) May, A. P.; Robinson, R. C.; Vinson, M.; Crocker, P. R.; Jones, E. Y. *Mol. Cell. Recogn.* **1998**, *1*, 719.
(55) Stehle, T.; Yan, Y.; Benjamin, T. L.; Harrison, S. C. *Nature* **1994**, *369*, 160.
(56) Eisen, M. B.; Sabesan, S.; Skehel, J. J.; Wiley, D. C. *Virology* **1997**, *232*, 19.
(57) Wright, C. S. *J. Mol. Biol.* **1990**, *215*, 635.
(58) Merritt, E. A.; Sarfaty, S.; van der Akker, F.; L'Hoit, C.; Martial, J. A.; Hol, W. G. J. *Prot. Sci.* **1994**, *3*, 166.
(59) Wymore, T.; Gao, X. F.; Wong, T. C. *J. Mol. Struct.* **1999**, *485*−*486*, 195.
(60) Tieleman, D. P.; van der Spoel, D.; Berendsen, H. J. C. *J. Phys. Chem.* **2000**, *104*, 6380S.
(61) Dill, K. A.; Flory, P. J. *Proc. Natl. Acad. Sci. (U.S.A.)* **1981**, *78*, 676.
(62) Kairash, A.; Boyd; B.; Lingwood, C. A. *J. Biol. Chem.* **1994**, *269*, 11138.
(63) Homans, S. W. *Glycobiology* **1993**, *3*, 551.
(64) Qasba, P. K.; Balaji, P. V.; Rao, V. S. R. *Glycobiology* **1994**, *4*, 805.
(65) Poveda, A.; Jimenez-Barbero, J. *Chem. Soc. Rev.* **1998**, *27*, 133.
(66) von der Lieth, C.-W.; Siebert, H.-C.; Kozar, T.; Burchert, M.; Frank, M.; Gilleron, M.; Kaltner, H.; Kayser, G.; Tajkhorshid, E.; Bovin, N. V.; Vliegenthart, J. F. G.; Gabius, H.-J. *Acta Anat.* **1998**, *161*, 91.